Influence of the Summer NAO on the Spring-NAO-Based Predictability of the East Asian Summer Monsoon

FEI ZHENG

State Key Laboratory of Numerical Modeling for Atmospheric Sciences and Geophysical Fluid Dynamics, Institute of Atmospheric Physics, Chinese Academy of Sciences, Beijing, China

JIANPING LI

College of Global Change and Earth System Science, Beijing Normal University, and Joint Center for Global Change Studies, Beijing, China

YANJIE LI

State Key Laboratory of Numerical Modeling for Atmospheric Sciences and Geophysical Fluid Dynamics, Institute of Atmospheric Physics, Chinese Academy of Sciences, Beijing, China

SEN ZHAO

State Key Laboratory of Numerical Modeling for Atmospheric Sciences and Geophysical Fluid Dynamics, Institute of Atmospheric Physics, Chinese Academy of Sciences, and University of Chinese Academy of Sciences, Beijing, China

DIFEI DENG

Key Laboratory of Cloud-Precipitation Physics and Severe Storms, Institute of Atmospheric Physics, Chinese Academy of Sciences, Beijing, China

(Manuscript received 16 July 2015, in final form 20 March 2016)

ABSTRACT

The dominant mode of atmospheric circulation over the North Atlantic region is the North Atlantic Oscillation (NAO). The boreal spring NAO may imprint its signal on contemporaneous sea surface temperature (SST), leading to a North Atlantic SST tripolar pattern (NAST). This pattern persists into the following summer and modulates the East Asian summer monsoon (EASM). Previous studies have shown that the summer NAST is caused mainly by the preceding spring NAO, whereas the contemporaneous summer NAO plays a secondary role. The results of this study illustrate that, even if the summer NAO plays a secondary role, it may also perturb summer SST anomalies caused by the spring NAO. There are two types of perturbation caused by the summer NAO. If the spring and summer NAO patterns have the same (opposite) polarities, the summer NAST tends to be enhanced (reduced) by the summer NAO, and the correlation between the spring NAO and EASM is usually stronger (weaker). In the former (latter) case, the spring-NAO-based prediction of the EASM tends to have better (limited) skill. These results indicate that it is important to consider the evolution of the NAO when forecasting the EASM, particular when there is a clear reversal in the polarity of the NAO, because it may impair the spring-NAO-based EASM prediction.

1. Introduction

Sea surface temperature (SST) variability in extratropical oceans is controlled mainly by physical processes near the ocean surface, such as surface heat

Corresponding author address: Dr. Fei Zheng, Institute of Atmospheric Physics, Chinese Academy of Sciences, Beijing 100029, China.
E-mail: zhengfei08@mail.iap.ac.cn

DOI: 10.1175/JAMC-D-15-0199.1

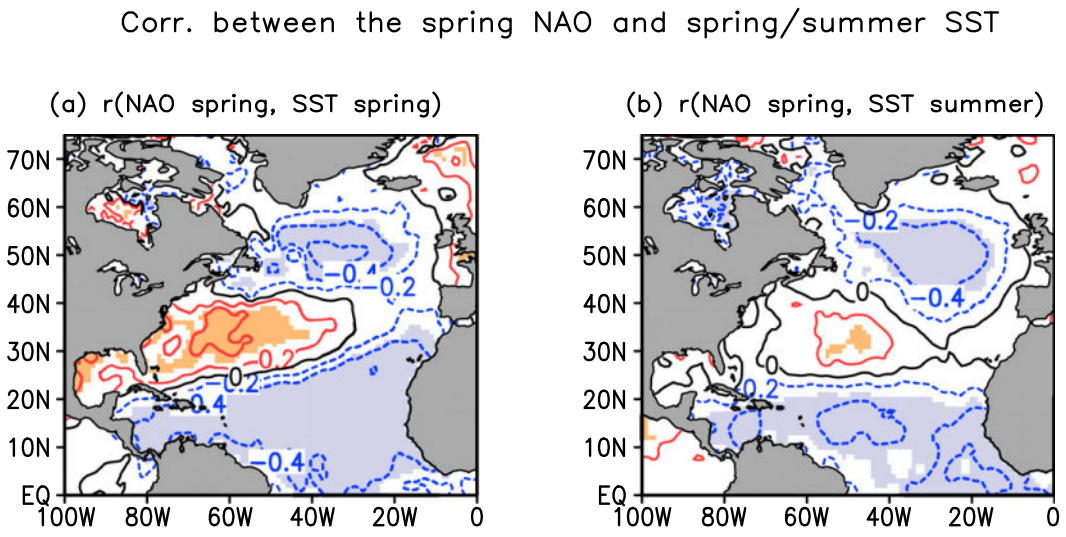

FIG. 1. Correlation coefficients between the spring NAO and (a) spring and (b) summer SSTs. The contour interval is 0.2, and color shaded areas indicate statistical significance at the 90% confidence level. The red (blue) contours represent positive (negative) values, and the black contours represent a correlation coefficient = 0.

exchange (e.g., sensible and latent heat flux) and Ekman transport (e.g., Xie 2004; Deser et al. 2010). As both the surface heat budget and Ekman transport are closely linked to variations in surface wind, extratropical SST variability is determined to a large extent by the overlying atmospheric circulation. The dominant modes of the extratropical atmospheric circulation emerge as large-scale meridional oscillations, such as the Northern Hemisphere annular mode (NAM; Thompson and Wallace 2000; Li and Wang 2003a), the North Atlantic Oscillation (NAO; Van Loon and Rogers 1978; Barnston and Livezey 1987; Li and Wang 2003b), and the Southern Hemisphere annular mode (SAM; Hartmann and Lo 1998; Gong and Wang 1999; Thompson and Wallace 2000; Li and Wang 2003a). Accordingly, extratropical SST anomalies tend to organize themselves into large-scale patterns (e.g., Xie 2004; Deser et al. 2010), such as the North Atlantic SST tripolar pattern (NAST; Marshall et al. 2001; Visbeck et al. 2003; Wu et al. 2009) in association with the NAO, and the Southern Hemisphere ocean dipole (SOD; Zheng et al. 2015a,b), which is related to the SAM.

Specifically, Figs. 1a and 1b show the correlation between the spring NAO and SST in spring and summer, respectively. It is evident that the spring NAO is closely linked to the NAST in spring (Fig. 1a). According to previous studies, the linkage between the spring NAO and NAST can be summarized as follows (e.g., Marshall et al. 2001; Visbeck et al. 2003; Xie 2004; Pan 2005; Wu et al. 2009; Deser et al. 2010; Zuo et al. 2012, 2013; Li et al. 2013). The NAO activity is accompanied by a north–south shift of the westerly jet. Specifically, when the NAO is in a positive (negative) phase, the jet shifts toward the Arctic (equator). Because of the quasi-barotropic feature of the NAO, surface wind speed also varies in phase with the upper-tropospheric jet stream. When prevailing winds over the extratropical oceans strengthen (weaken), local SST tends to be cooler (warmer) because of the increased (decreased) loss of heat and anomalous cooler (warmer) Ekman heat transport (e.g., Xie 2004; Deser et al. 2010). Generally, enhanced (reduced) surface wind speed often favors cold (warm) SST anomalies (e.g., Xie 2004; Deser et al. 2010). Therefore, spring SST anomalies over the North Atlantic Ocean exhibit a tripolar pattern in response to the surface wind speed distribution associated with the spring NAO. Although other physical processes such as internal ocean dynamics may also contribute to summer SST variability, the spring NAO plays a key role in the formation of the NAST pattern.

It is well known that seawater is characterized by strong persistence because of its large heat capacity (e.g., Deser et al. 2003). Hence, extratropical SST anomaly patterns (e.g., the NAST and SOD) caused by large-scale atmospheric modes (e.g., the NAO and SAM) can span across seasons. The spring NAST, caused by the contemporaneous NAO, can persist into the following summer (Fig. 1b; Wu et al. 2009; Zuo et al. 2012, 2013). The cross-seasonal influence of the spring NAO on the summer NAST is attributed mainly to the persistence of SST anomalies that originate in spring (e.g., Wu et al. 2009).

In summer, the NAST may trigger an Atlantic–Europe–Asia (AEA) teleconnection over Eurasia. The mechanism for maintaining the AEA wave train pattern involves both

anomalous diabatic heating and synoptic eddy-vorticity forcing (Zuo et al. 2012, 2013). The AEA teleconnection contains a cyclonic circulation center over the Ural Mountains, which is found to play a critical role in influencing the East Asian summer monsoon (EASM) by previous studies (Zhang and Tao 1998; Li and Ji 2001; Wu et al. 2009, 2012; Zuo et al. 2012, 2013; Li et al. 2013). Therefore, the spring NAO imprints its signal on the North Atlantic summer SST, which triggers the AEA teleconnection and provides a source of predictability for the EASM. A significant positive correlation exists between the spring NAO and EASM. A positive (negative) phase of the spring NAO is usually followed by a strong (weak) EASM year. Wu et al. (2009) established an empirical model to predict the EASM based on a combination of the spring NAO and El Niño–Southern Oscillation (ENSO), and showed that the performance of this empirical model is comparable to the ensemble hindcast by multinumerical models, and that the spring NAO indeed provides a source of predictability for the EASM.

Except for the spring NAO, the summer NAO can also influence the summer North Atlantic SST and lead to a similar tripolar-like SST anomaly pattern over the North Atlantic (e.g., Wu et al. 2009; Zuo et al. 2012, 2013; Xu et al. 2013). Hence, the summer SST field over the North Atlantic contains anomalies caused by both the spring and summer NAO. If the spring NAO plays a dominant role in influencing the summer SST, the spring NAO and associated SST anomalies can be regarded as effective predictors for the EASM. However, if the summer NAO plays a dominant role, summer SST anomalies caused by the spring NAO are modulated to a great extent by the summer NAO and, thus, affect the predictability of the EASM.

To detect the relative importance of the spring and summer NAO in driving the summer NAST, Wu et al. (2009) carried out a decomposition of summer SST using a unary linear regression method, in which the dependent variable is summer SST and the independent variable is spring SST. Using this method, summer SST is decomposed to a persistent component derived from spring SST and a nonpersistent component independent of spring SST (see also Pan 2005). The decomposition shows that summer NAST is mainly caused by the preceding spring NAO, while the contemporaneous summer NAO plays a secondary role (Wu et al. 2009).

Nevertheless, even if the spring NAO plays a larger role than the summer NAO in influencing North Atlantic summer SST, SST anomalies caused by the spring NAO would still be perturbed by the summer NAO. Little attention has been paid to this kind of perturbation. Since North Atlantic summer SST acts as an important ''bridge'' in the cross-seasonal influence of the spring NAO on the EASM, perturbations of summer SST by the summer NAO would further affect the spring-NAO-based predictability of EASM. However, less is known about the influence of summer NAO on the linkage between the spring NAO and EASM. Since the EASM is significantly correlated with summer rainfall in East Asia, including the middle and lower reaches of the Yangtze River in China, southern Japan, and the Maritime Continent (Wang 2001; Ding and Chan 2005; Wu et al. 2009; Wu and Yu 2015; Gong et al. 2011; An et al. 2015; Chen et al. 2015), EASM predictions provide an important basis for seasonal predictions of East Asian summer precipitation. Therefore, understanding the predictability of the EASM is of great importance.

The aim of this paper is to detect the influence of the summer NAO on summer SST anomalies related to the spring NAO, and explore the consequent effects on the seasonal prediction of the EASM. The remainder of the manuscript is organized as follows. The data and methodology adopted in this study are described in section 2. Section 3 investigates the modulation of summer SST anomalies by the summer NAO. On this basis, section 4 explores the influence of the summer NAO on the predictability of the EASM. A discussion and conclusions are presented in section 5.

2. Data and methodology

a. Data

Atmospheric circulation data are employed from the National Centers for Environmental Prediction–National Center for Atmospheric Research (NCEP–NCAR) reanalysis with a horizontal resolution of 2.5° × 2.5°. The SST dataset is the National Oceanic and Atmospheric Administration (NOAA) Extended Reconstructed SST (ERSST), version 3b (V3b), with a horizontal resolution of 2.5° × 2.5°. This study focuses on boreal spring (March–May) and summer (June–August) for the period 1979–2012. Unless otherwise stated, all meteorological parameters were converted to seasonal means prior to regression or correlation analyses.

The Niño-3.4 index, defined as the regionally averaged SST over 5°S–5°N and 170°–120°W, is used to represent ENSO variability. The monthly Niño-3.4 index derived from ERSST is available from the NOAA Climate Prediction Center (CPC; http://www.cpc.ncep.noaa.gov/data/indices/). The variability of the NAO is quantified by the NAO index, defined as the difference between the normalized monthly sea level pressure (SLP) over the North Atlantic sector averaged from

80°W to 30°E at 35°N and that at 65°N (Li and Wang 2003b).

b. EASM index

A unified dynamic normalized seasonality (DNS) monsoon index reported by Li and Zeng (2000, 2002) is applied to delineate the magnitude and variability of the EASM. The DNS index is expressed as follows:

$$\delta_{nm}(i,j) = \frac{\|\overline{\mathbf{V}}_1(i,j) - \mathbf{V}_{nm}(i,j)\|}{\|[\overline{\mathbf{V}}_1(i,j) + \overline{\mathbf{V}}_7(i,j)]/2\|} - 2, \qquad (1)$$

where $\overline{\mathbf{V}}_1(i, j)$ and $\overline{\mathbf{V}}_7(i, j)$ are the January and July climatology wind vectors, respectively, and $\mathbf{V}_{nm}(i, j)$ is the wind vector at grid point (i, j) in the mth month–day of the nth year.

The DNS index is based on wind field seasonality intensity, and can be used to depict the seasonal cycle and interannual variability of the monsoon over different regions (Feng et al. 2010; Shi et al. 2014; An et al. 2015; Feng et al. 2015; Li et al. 2015; Zhao et al. 2015). A large-scale monsoon index can be defined as the area-averaged DNS index over a specific monsoon domain at a certain altitudinal level. The EASM index adopted in this study is defined as an area-averaged summer (June–August) DNS index at 850 hPa within the East Asian monsoon domain (10°–40°N, 110°–140°E).

Another EASM index proposed by Wang and Fan (1999) is also adopted in this study, and is defined by the summer (June–August) zonal wind at 850 hPa averaged across 22.5°–23.5°N, 110°–140°E minus that averaged across 5°–15°N, 90°–130°E. Variations of the two EASM indices (Wang and Fan 1999; Li and Zeng 2000, 2002; Wang et al. 2008; Wu and Yu 2015) are in close agreement, with a correlation coefficient of 0.92 for the period 1979–2012.

c. Statistical method

The primary statistical tools used in the present study are regression and correlation analyses. The NAO and EASM indices are standardized before regression analysis so that the regression coefficients represent circulation anomalies corresponding to one standard deviation of the NAO and EASM indices. A Student's t test is employed to assess the statistical significance of the correlation and regression coefficients between two variables x and y using effective degrees of freedom (denoted as N), which is based on Davis (1976) and Chen (1982) and is expressed as

$$N = n/T, \qquad (2)$$

$$T = \sum_{\tau=1}^{\tau=\text{lag}} R_{xx}(\tau) \times R_{yy}(\tau), \qquad (3)$$

$$R_{xx}(\tau) = \frac{1}{n-\tau} \sum_{t=1}^{n-\tau} x_t^* \times x_{t+\tau}^*, \quad \text{and} \qquad (4)$$

$$R_{yy}(\tau) = \frac{1}{n-\tau} \sum_{t=1}^{n-\tau} y_t^* \times y_{t+\tau}^*, \qquad (5)$$

where the lag in Eq. (3) is usually taken as one-half of n and the superscript asterisk in Eqs. (4) and (5) indicates standardized variables.

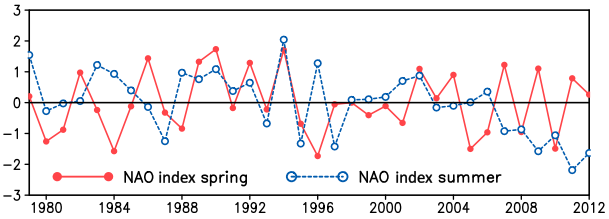

FIG. 2. Normalized time series of spring (red) and summer (blue) NAO indices.

d. Method for detecting perturbation by the summer NAO

Figure 2 shows the normalized time series of the spring and summer NAO. For the entire analysis period (1979–2012), there are 16 yr in which the summer NAO has the same sign as the spring NAO, and 18 yr in which the summer NAO has an opposite sign to the spring NAO. The above two cases are referred to as "same sign" and "opposite sign" scenarios hereafter, and the same-sign and opposite-sign years during 1979–2012 are listed in Table 1.

The occurrence of same-sign and opposite-sign scenarios is almost equivalent for the analysis period. That is, when the spring NAO is in a positive (negative) phase, the probability of the occurrence of positive and negative NAO patterns in the following summer is

TABLE 1. List of the same-sign and opposite-sign years. Same-sign and opposite-sign years are categorized by the summer NAO having the same or opposite polarity to the spring NAO, respectively. In the analysis period 1979–2012, there are 16 same-sign and 18 opposite-sign years.

Scenarios	Years
Same sign (16 yr)	1979, 1980, 1981, 1982, 1987, 1989, 1990, 1992, 1993, 1994, 1995, 1997, 1998, 2002, 2008, 2010
Opposite sign (18 yr)	1983, 1984, 1985, 1986, 1988, 1991, 1996, 1999, 2000, 2001, 2003, 2004, 2005, 2006, 2007, 2009, 2011, 2012

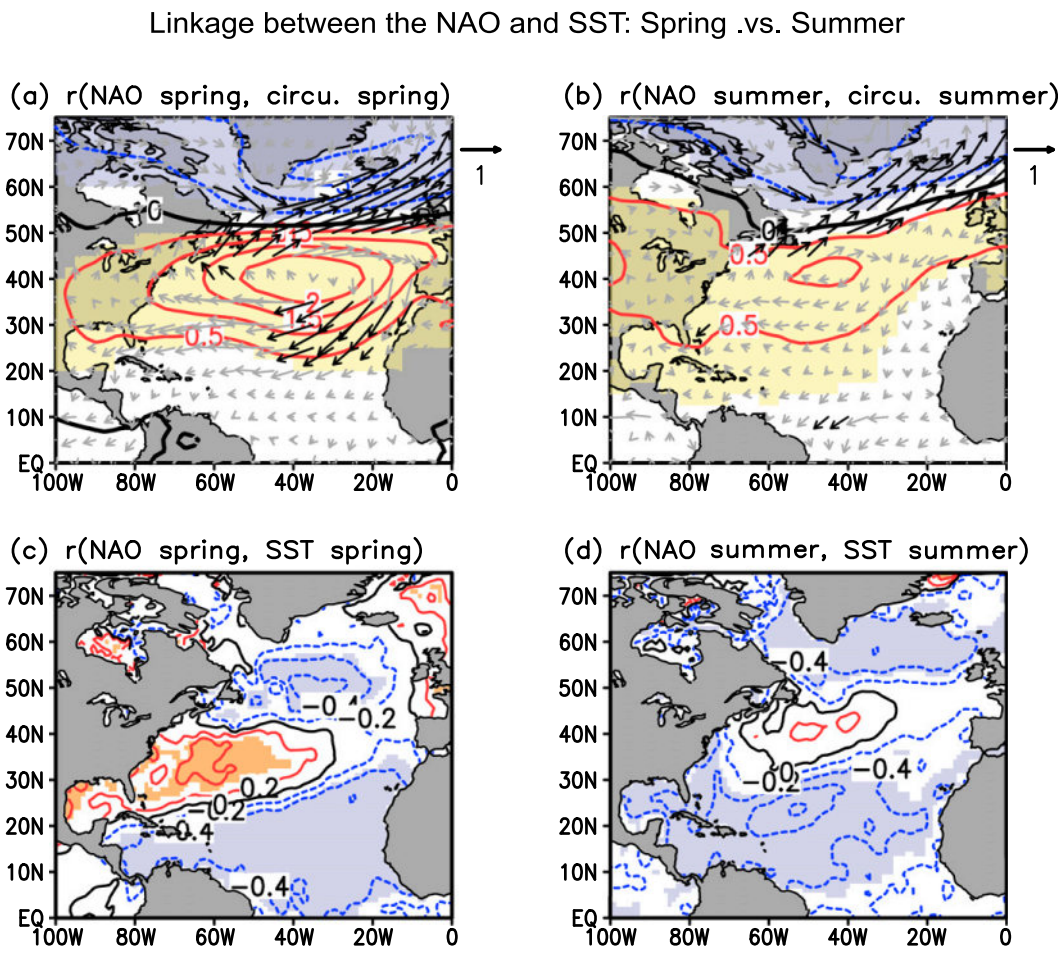

FIG. 3. (a) Regression of spring SLP (contour interval = 0.5 hPa) and horizontal wind (vectors; m s^{-1}) at 850 hPa against the spring NAO index. Black vectors are statistically significant at the 90% confidence level. (b) As in (a), but for summer. (c) Correlation coefficients between the spring NAO and spring SST (contour interval = 0.2) as in Fig. 1a. (d) As in (c), but for summer. Red (blue) contours represent positive (negative) values, and the black contours represent a correlation coefficient = 0. Color-shaded areas indicate statistical significance at the 90% confidence level.

almost equivalent. In addition, since the spring and summer NAO indices were normalized before correlation analysis, their correlation coefficient can also be viewed as a reflection of the ratio of the same polarities between the two variables. If the correlation coefficient is a significantly positive (negative) value, there tends to be more same-sign (opposite sign) cases between the two variables. The correlation between the spring and summer NAO during 1979–2012 is almost zero (0.05), implying the quasi equivalence of the same-sign and opposite-sign scenarios, which is consistent with Table 1.

In the following analyses, the connections between the spring NAO and summer North Atlantic SST–EASM–summer atmospheric circulation pattern are explored separately using the same-sign and opposite-sign years listed in Table 1. The term "raw results" refers to the results using all samples in the entire 34-yr period (1979–2012). The raw results can be viewed as not being influenced by the summer NAO, since they contain years in both of the above two scenarios, which cancel out the effect of the summer NAO. The difference between the results in the same-sign (opposite sign) scenario and the raw results can be viewed as the influence of the same-sign (opposite sign) summer NAO on the connections between the spring NAO and North Atlantic SST–EASM–summer atmospheric circulation pattern.

3. Modulation of summer SST anomalies by the summer NAO

The spatial pattern of the spring NAO is shown in Fig. 3a. This is calculated by regressing SLP against the spring NAO index. The NAO manifests itself as a

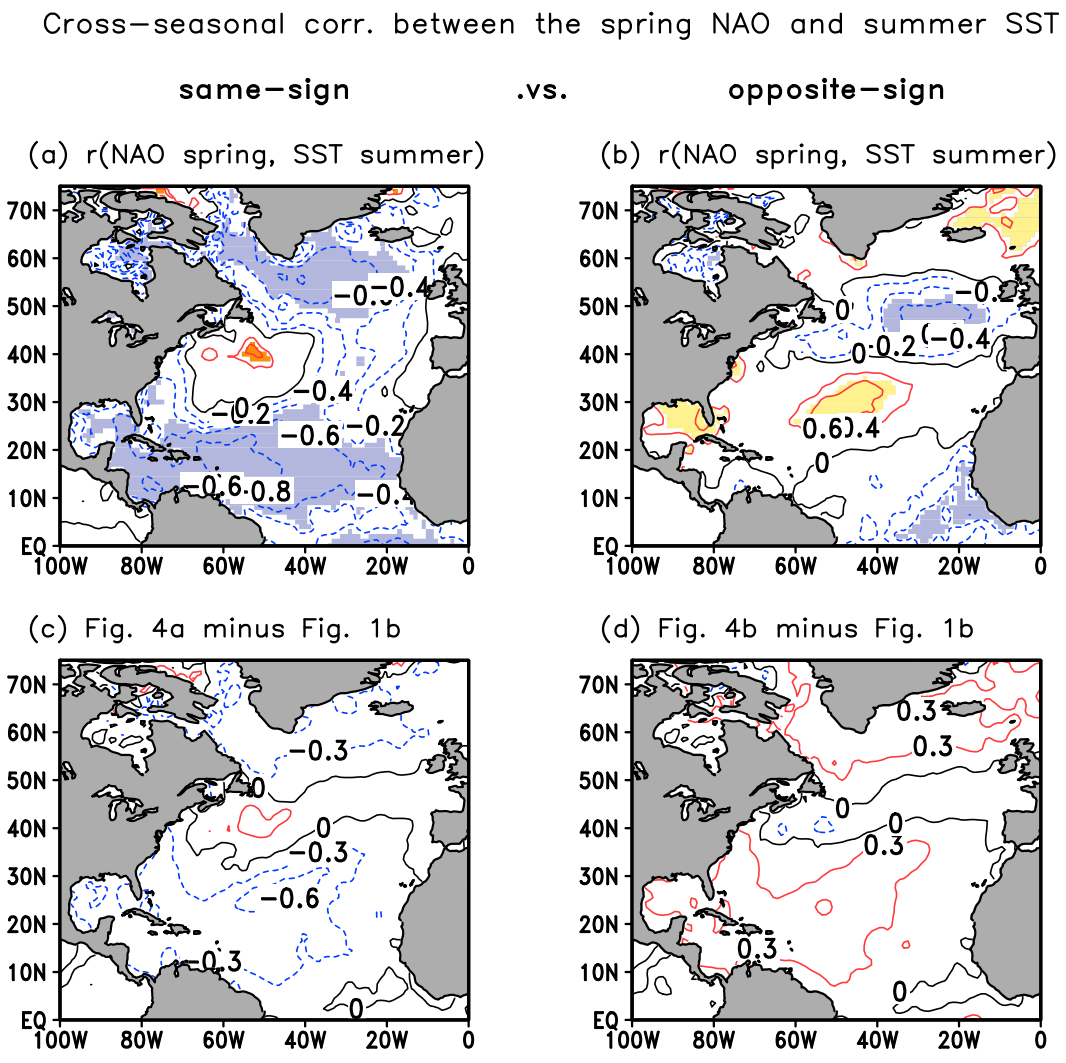

FIG. 4. (a) Correlation coefficients between the spring NAO and summer SST for the same-sign scenario (years when the summer NAO has the same polarity as the spring NAO). The contour interval is 0.2. The red (blue) contours represent positive (negative) values, and black contours represent a correlation coefficient = 0. Color-shaded areas represent statistical significance at the 90% confidence level. (b) As in (a), but for the opposite-sign scenario (years when the summer NAO has an opposite polarity to the spring NAO). (c) Difference between (a) and Fig. 1b, and (d) difference between (b) and Fig. 1b; contour interval = 0.3.

seesaw of SLP between the Arctic and middle latitudes of the Atlantic sector (e.g., Van Loon and Rogers 1978; Barnston and Livezey 1987; Li and Wang 2003b). Specifically, when the NAO is in a positive (negative) phase, the polar low is stronger (weaker), while SLP at middle latitudes is higher (lower). This oscillation in SLP is accompanied by changes in horizontal wind across the North Atlantic, with anomalous cyclonic and anticyclonic circulation patterns at high and middle latitudes, respectively. Circulation anomalies related to the summer NAO (Fig. 3b) are generally consistent with those in spring (Fig. 3a), but are relatively weak with the strength of the geopotential height anomalies in the middle latitudes being only half that of spring (Fig. 3a).

Previous studies have separately investigated the correlation coefficient distributions between North Atlantic SST and the contemporaneous NAO in spring and summer, using different SST datasets and analysis periods (e.g., Wu et al. 2009; Xu et al. 2013). Here, we show them together in Figs. 3c,d to make a clear comparison between them. Because of the similarity between the spring and summer NAO signals (Figs. 3a,b), SST anomalies in spring and summer related to the contemporaneous NAO also show similar NAST characteristics (Figs. 3c,d). These SST anomalies include a tripolar structure marked by a cold anomaly in the subpolar North Atlantic, a warm anomaly in the middle latitudes, and a cold subtropical anomaly at low

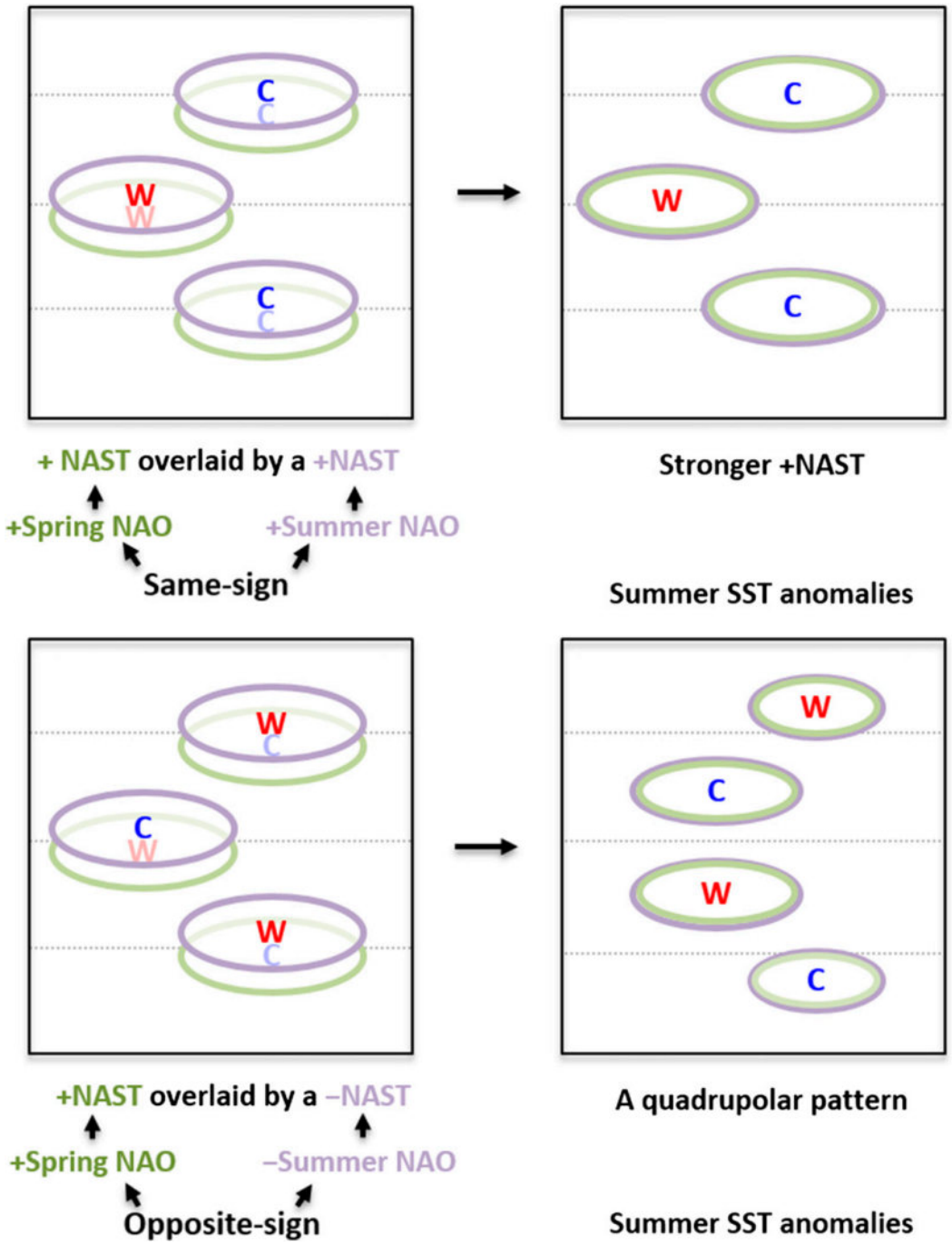

FIG. 5. Schematic showing the overlay of summer NAST related to the summer NAO on summer NAST related to the spring NAO. The (top) same-sign and (bottom) opposite-sign scenarios are shown. (left) The summer NAST associated with the summer NAO is displayed at the top layer (purple lines), and the summer NAST associated with the spring NAO is shown at the bottom layer (green lines). (right) The total SST anomalies after the overlay; the overlay contains anomalies related to both the spring and summer NAO. The ellipses marked by the red W and blue C indicate warm and cold SST anomalies, respectively. Note that the summer NAST related to the summer NAO is located farther north than that related to the spring NAO.

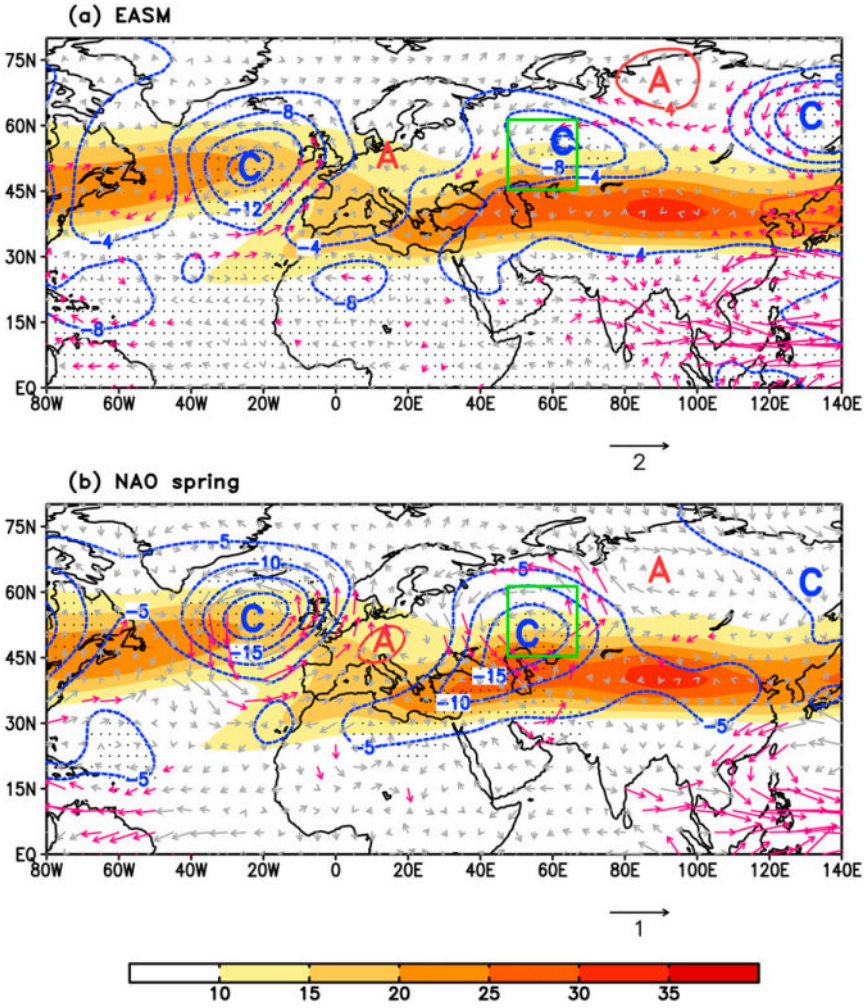

FIG. 6. Regression of summer geopotential height (contour interval = 5 gpm) at 200 hPa and horizontal wind (vectors; m s^{-1}) at 850 hPa against the (a) EASM and (b) spring NAO indices. The stippling and red vectors represent statistical significance at the 95% confidence level for the contours and vectors, respectively. Colored shading represents the climatological summer zonal wind > 10 m s^{-1}, which generally reflects the position of the westerly jet. The letters A and C indicate anomalous positive (anticyclonic) and negative (cyclonic) centers in the geopotential height field at 200 hPa, respectively. The Ural Mountains region is marked with the green box.

latitudes, all of which are consistent with previous studies (e.g., Marshall et al. 2001; Deser et al. 2003, 2010; Visbeck et al. 2003; Wu et al. 2009; Zuo et al. 2012, 2013; Xu et al. 2013).

However, Figs. 3c,d also show some differences. For example, the middle-latitude warm center related to the summer NAO is weaker (Fig. 3d) than that related to the spring NAO (Fig. 3c), which may be partially attributed to the responses of the atmospheric circulation to the summer NAO being weaker than those for the spring NAO. In addition, the NAST in summer (Fig. 3d) is located farther north in comparison with that in spring (Fig. 3c). The two cold centers in high and low latitudes and the middle-latitude warm center of the NAST are located at around 50°, 15°, and 35°N, respectively, in spring. In summer, the three centers all shift north and are located at around 60°, 25°, and 40°N, respectively. In general, the summer NAST pattern is about 10° farther north than that in spring. A careful comparison between Figs. 3a,b suggests that the NAO pattern itself also exhibits a northward shift in summer. The northward shift of the summer NAST may be related to the northward shift of the NAO, despite the fact that the amplitude of the NAO shift is smaller than that of the NAST.

The influence of the summer NAO on summer SST anomalies caused by the spring NAO may be divided

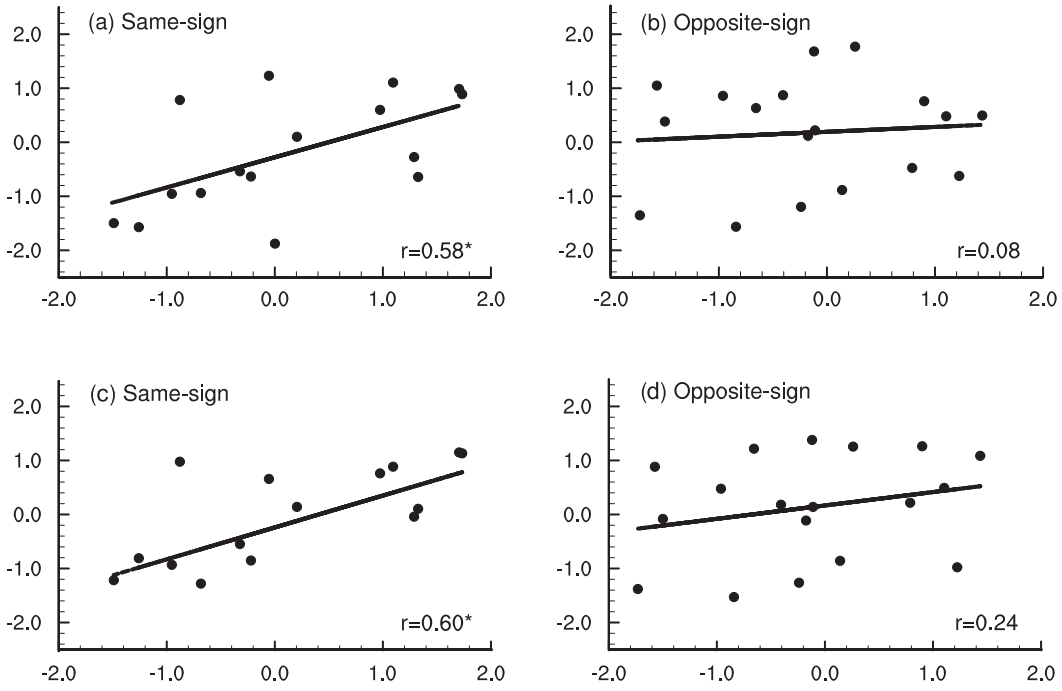

FIG. 7. Scatterplot of the EASM index reported by (a),(b) Li and Zeng (2000, 2002) and (c),(d) Wang and Fan (1999) against the spring NAO index for the (left) same-sign and (right) opposite-sign scenarios. The corresponding correlation coefficients are provided at the bottom-right corners of the panels. The asterisk indicates statistical significant at the 95% confidence level.

into same-sign and opposite-sign cases (see section 2d). Figure 4a shows correlation coefficients between the spring NAO and summer SST for the same-sign scenario. It is clear that the cold centers at high and low latitudes are stronger than the raw results in Fig. 1b. The difference between Figs. 4a and 1b is shown in Fig. 4c, which is used to quantitatively illustrate the influence of the same-sign summer NAO on summer SST anomalies caused by the spring NAO. It is clear in Fig. 4c that the same-sign scenario generally enhances the strength of the NAST pattern. Specifically, cold centers at high and low latitudes are colder, while the warm center in the middle latitudes is warmer. This is because SST anomalies caused by the spring NAO are enhanced by the same-sign summer NAO. In addition, the tripolar pattern in Fig. 4a is located slightly north of that in Fig. 1b. For example, the three anomaly centers from north to south in Fig. 1b are located at around 50°, 35°, and 15°N, respectively, while those in Fig. 4a are located at around 55°, 40°, and 18°N, respectively. This difference in the position of the centers is related to the fact that the summer-NAO-based NAST shifts farther north than does the spring-NAO-based NAST (Figs. 3c,d).

Figure 4b shows the correlation coefficients between the spring NAO and summer SST for the opposite-sign scenario. Although regions of significant correlation do exist, the tripolar pattern has been disturbed and resembles a quadrupolar pattern. Figure 4d shows the difference between Figs. 4b and 1b. It is clear in Fig. 4d that, when compared with the raw results, the cold centers in the high and low latitudes are warmer, and the warm center in the middle latitudes is colder. This result implies that the NAST pattern is weakened by the summer NAO in the opposite-sign scenario.

Figure 5 shows a schematic illustrating the influence of the summer NAO on summer SST anomalies. In short, the summer NAO does indeed play a role in affecting summer SST anomalies caused by the spring NAO, and perturbations by the summer NAO are different for the same-sign and opposite-sign scenarios. The same-sign summer NAO generally enhances the NAST pattern caused by the spring NAO, whereas in the opposite-sign scenario the NAST pattern is weakened by the opposite-sign summer NAO and a quadrupolar pattern emerges.

4. Modulation of EASM predictability by the summer NAO

The spring NAO provides a degree of predictability for the EASM by imprinting its signal on the North Atlantic summer SST (e.g., Wu et al. 2009; Zuo et al.

2012, 2013). The results presented above clearly show the different influences of the summer NAO on summer SST anomalies caused by the spring NAO for same-sign and opposite-sign scenarios. Thus, it is inferred that the summer NAO may also perturb the predictability of the EASM based on the spring NAO.

Figure 6 shows some basic aspects of the influence of the spring NAO on EASM by regressing the summer circulation anomalies against the EASM and the spring NAO indices, including geopotential height at 200 hPa and horizontal wind at 850 hPa. The circulation anomalies in Figs. 6a,b show a high degree of consistency, suggesting a close linkage between the spring NAO and EASM. For example, a systematic wave train pattern prevails along the poleward flank of the westerly jet at 200 hPa. This wave train pattern is referred to as the North Atlantic–Eurasia teleconnection (Zuo et al. 2013) or AEA (Wu et al. 2009; Li et al. 2013), which is characterized by three negative centers over the North Atlantic, Ural Mountains, and Okhotsk Sea, and two relatively weak positive centers over western Europe and Mongolia. The AEA exhibits an equivalent barotropic structure throughout the entire troposphere and, thus, is also reflected in the horizontal wind field at 850 hPa. In addition, an anomalous cyclonic circulation with enhanced northeasterly winds on its northwest flank exists at 850 hPa over the western Pacific Ocean and East Asia.

The summer NAST pattern acts as a ''bridge'' in the cross-seasonal influence of the spring NAO on the EASM. The triggering role of the summer NAST on the AEA teleconnection has been verified in numerical model simulations (Wu et al. 2009; Zuo et al. 2012, 2013; Li et al. 2013). In the AEA teleconnection, geopotential height anomalies over the Ural Mountains play an important role in influencing the EASM. Cyclonic circulation anomalies over the Ural Mountains represent reduced blocking activity over this region, which favors a weakened East Asian subtropical front and tends to result in a stronger EASM (Zhang and Tao 1998; Li and Ji 2001; Zuo et al. 2013). Cyclonic circulation anomalies over the Ural Mountains coincide with the positive phase of the spring NAO, and agree with the in-phase relationship between the spring NAO and EASM (Wu et al. 2009; Zuo et al. 2012, 2013).

Scatterplots of the EASM index against the spring NAO index for the same-sign and opposite-sign scenarios are shown in Figs. 7a and 7b, respectively. When the spring NAO has the same polarity as the summer NAO, a significant positive correlation with a correlation coefficient of 0.58 exists between the EASM and spring NAO (Fig. 7a). Conversely, when the spring NAO has the opposite polarity to the summer NAO, there is almost no significant correlation between the EASM and spring NAO (Fig. 7b). The stronger linkage between the spring NAO and EASM in the same-sign scenario than in the opposite-sign scenario results from the stronger correlation in the same-sign scenario between the spring NAO and summer NAST.

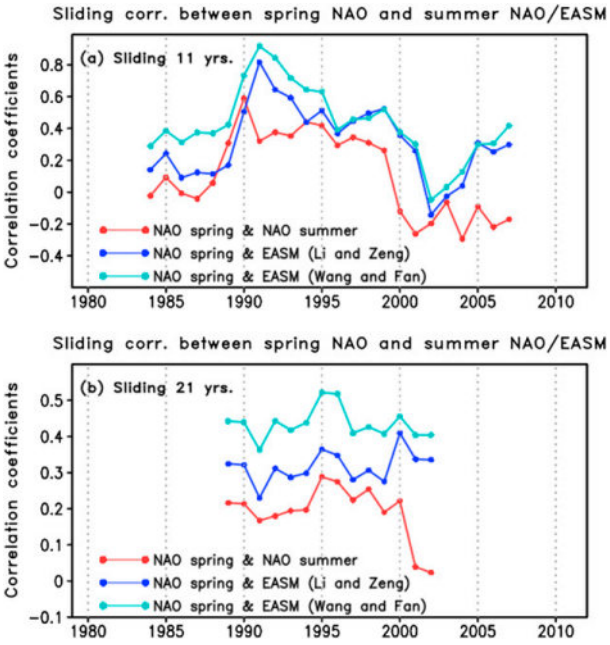

FIG. 8. The (a) 11- and (b) 21-yr sliding correlations between the spring and summer NAO (red line) and the spring NAO and EASM (blue and cyan lines). Results derived from the EASM index follow the definition of Li and Zeng (2000, 2002) or Wang and Fan (1999) and are shown by blue and cyan lines, respectively.

To validate the results in Figs. 7a,b, similar analysis based on another EASM index (Wang and Fan 1999; Wang et al. 2000, 2008) was carried out and the results are shown in Figs. 7c,d. The correlation coefficients in the same-sign and opposite-sign scenarios based on the Wang and Fan (1999) EASM index are 0.60 (significant at the 95% confidence level) and 0.24 (not significant even at the 20% confidence level), respectively. A comparison between Figs. 7c and 7d also suggests that the relationship between the spring NAO and EASM is stronger in the same-sign scenario than in the opposite-sign scenario, which is consistent with the results based on the EASM index of Li and Zeng (2000, 2002).

Figure 8a shows 11-yr sliding correlations between the spring and summer NAO (red line). As in section 2d, because the spring and summer NAO patterns were both normalized before correlation analysis, the correlation coefficient can be viewed as a reflection of the ratio of the same polarity in each variable. The autocorrelation between the spring and summer NAO is

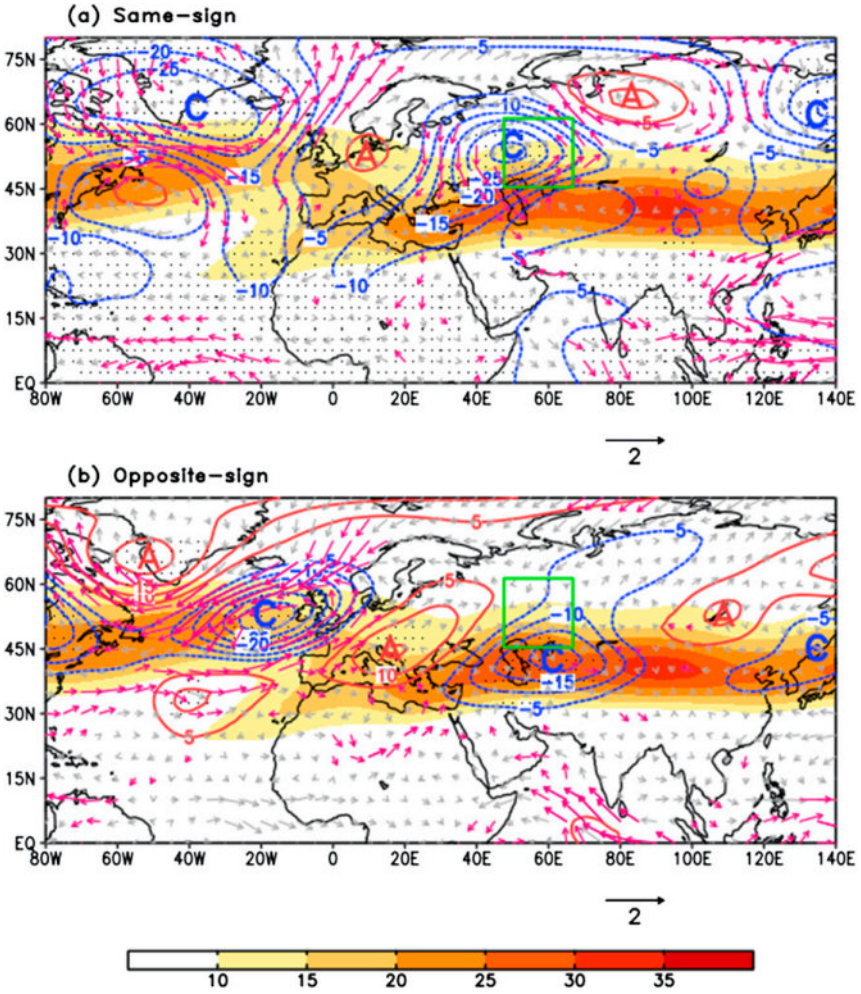

FIG. 9. As in Fig. 6b, but for the (a) same-sign and (b) opposite-sign scenarios.

almost zero during the analysis period (1979–2012), suggesting the quasi-equivalence of the same-sign and opposite-sign scenarios during 1979–2012. The 11-yr correlation between the spring and summer NAOs is used to reflect the ratio of the same-sign scenario during the sliding window. The relatively high (low) autocorrelation suggests that there tends to be more same-sign (opposite sign) cases during the 11-yr sliding window. Also shown in Fig. 8a are the 11-yr sliding correlations between the spring NAO and EASM based on both EASM definitions (cyan and blue lines) (Wang and Fan 1999; Li and Zeng 2000, 2002; Wang et al. 2000, 2008). Variations in the three curves in Fig. 8a are generally consistent and show that a stronger (weaker) correlation between the spring and summer NAO patterns during the sliding window results in more same-sign (opposite sign) spring and summer NAO polarities, and a stronger (weaker) relationship between the spring NAO and EASM.

Figure 8b shows a similar analysis, but for correlations obtained using a 21-yr moving window. Similarly, the variations in the curves are generally in agreement. The stronger the correlation between the spring and summer NAO, the stronger the correlation between the spring NAO and EASM. These results suggest robustness in the influence of summer NAO on the linkage between the spring NAO and EASM.

Further evidence for the influence of summer NAO on the linkage between the spring NAO and summer circulation is given in Figs. 9a,b. Contours show the regression of the summer geopotential height anomalies at 200 hPa against the spring NAO index in the same-sign and opposite-sign scenarios, respectively. The AEA teleconnection is clearly evident in the same-sign case, and prevails along the poleward flank of the westerly jet. However, in the opposite-sign case (Fig. 9b), the teleconnection over Eurasia exhibits obvious differences from the AEA teleconnection. The wave train pattern in

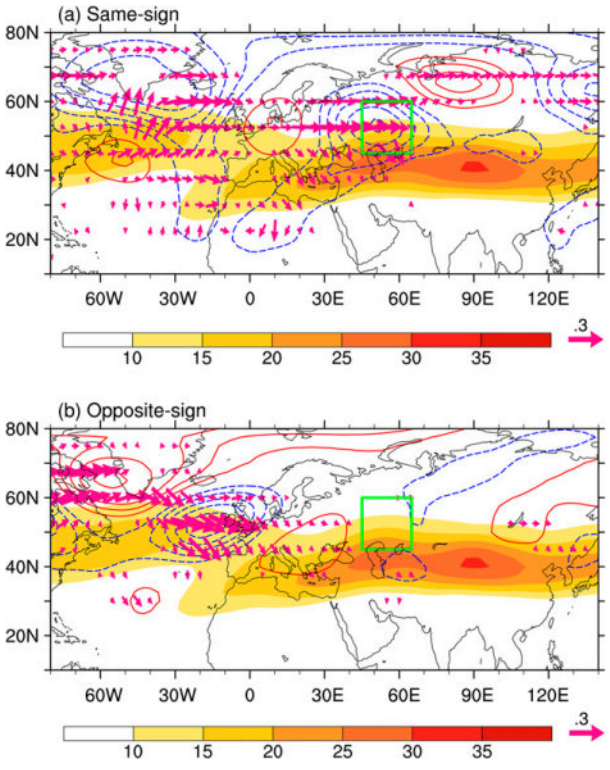

FIG. 10. (a) Regression of summer geopotential height anomalies at 500 hPa (contour interval = 5 gpm) and the associated wave activity flux (vectors; $m^2 s^{-2}$) against the spring NAO index for the same-sign scenario. The red (blue) contours represent positive (negative) values. Colored shading represents the climatological summer zonal wind $> 10 m s^{-1}$. The Ural Mountains region is marked with the green box. (b) As in (a), but for the opposite-sign scenario.

this case propagates mainly in the jet stream, while the AEA prevails along the poleward flank of the jet.

Differences also exist in the strength of the teleconnection in each scenario. In the same-sign scenario, the teleconnection is generally stronger than in the opposite-sign scenario, and appears in both the lower (850 hPa) and middle troposphere (500 hPa). For example, horizontal wind anomalies at 850 hPa in the three AEA teleconnection centers (negative centers over the Ural Mountains and Okhotsk Sea, and the positive center over Mongolia) are clearly significant in Fig. 9a, while those in Fig. 9b are not significant and almost disappear. In addition, regressed geopotential height anomalies at 500 hPa and the associated wave activity flux shown in Fig. 10 show clearly that the wave activity over Eurasia is more prominent in the same-sign scenario than in the opposite-sign scenario.

It is well known that atmospheric teleconnections are a representation of energy transport and wave propagation. Differences in wave source will lead to changes in the teleconnection pattern (e.g., Frederiksen and Webster 1988; Trenberth et al. 1998; Liu and Alexander 2007; Li et al. 2015; Zhao et al. 2015). The wave source is generally indicated by the divergence of the wave activity flux (Takaya and Nakamura 2001). As shown in Fig. 10, the wave source over the North Atlantic in the same-sign case is mainly located in the region 30°–50°N, 70°–30°W, while that in the opposite-sign case is mainly located in the region 40°–60°N, 30°W–0°. The stationary Rossby wave ray paths starting from the above two wave sources based on the same background flow derived from the summer climatology are given in Figs. 11a and 11b, respectively.

The wave ray path is a trajectory that is locally tangential to the group velocity vector (Lighthill 1978) and, thus, can be used to quantitatively represent the behavior of energy. A detailed description of the wave ray equations and the calculation of Rossby wave ray paths based on the barotropic nondivergent vorticity equation on a time-mean slowly varying basic state can be found in Li et al. (2015) and Zhao et al. (2015). Figure 11 shows that Rossby wave ray paths in the same-sign scenario mainly propagate westward along the poleward flank of the jet and pass the centers in the AEA teleconnection. In the opposite-sign scenario, the majority of ray paths are limited to the jet stream, implying the refraction of the wave and the waveguide's role in the jet. The results from the analysis of the wave activity flux in Fig. 10 and Rossby wave ray paths in Fig. 11 verify the results in Fig. 9. It can be deduced that the summer NAO modulates the downstream propagation of initial circulation anomalies.

As mentioned above, geopotential height anomalies over the Ural Mountains in the AEA teleconnection play an important role in influencing the EASM. In the same-sign scenario, there is a significant wave activity flux (Fig. 10a) and significant cyclonic circulation anomalies (Fig. 9a) around the Ural Mountains. In the opposite-sign scenario, the wave activity flux around the Ural Mountain is very weak (Fig. 10b), and cyclonic circulation anomalies are also relatively small (Fig. 9b).

Cyclonic circulation anomalies over the Ural Mountains favor a weakened East Asian subtropical front that tends to result in a stronger EASM (Zhang and Tao 1998; Li and Ji 2001; Zuo et al. 2013). Figure 12a shows that a weak EASM is indeed clearly linked to a weakened East Asian subtropical jet. In the same-sign case (Fig. 12b), because of the significant cyclonic circulation anomalies over the Ural Mountains, the East Asian subtropical jet weakens and further contributes to a stronger EASM. In contrast, the East Asian subtropical jet does not weaken in the opposite-sign case (Fig. 12c) because of the relatively small cyclonic circulation

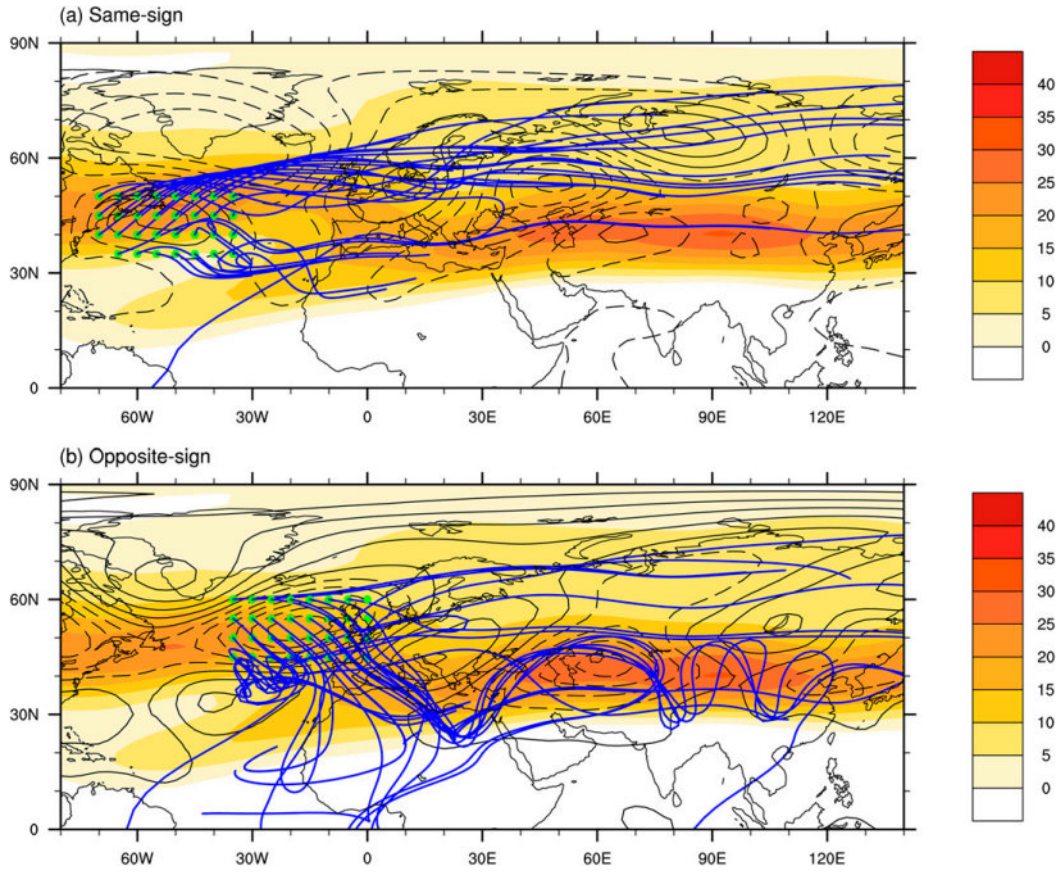

FIG. 11. Stationary Rossby wave ray paths (blue lines) starting from different source regions (green dots) according to the height anomalies at 200 hPa (contour interval = 5 gpm) in the (a) same-sign and (b) opposite-sign scenarios. Rays are initiated with zonal wavenumber 3 and integrated 400 times with an interval of 1 h using the fourth-order Runge–Kutta method. The background flow is derived from the smoothed June–August climatology using a two-dimensional Fourier series truncated at zonal and meridional wavenumber 8, and the starting points (green dots) are identified from the wave activity flux divergence. Plots of the ray paths are superimposed on the distribution of the climatological zonal wind (color shading; m s^{-1}).

anomalies over the Ural Mountains, which provides an explanation for the weak correlation between the spring NAO and EASM in this case. Meanwhile, atmospheric cyclonic circulation at 850 hPa over the western Pacific is also strengthened in the same-sign scenario (Fig. 9a) in comparison with that in the opposite-sign scenario (Fig. 9b), which is in agreement with the stronger correlation between the spring NAO and EASM in the same-sign scenario.

In view of the influence of the summer NAO on the linkage between the spring NAO and EASM patterns, it is expected that the predictability of EASM based on the spring NAO may also be affected by the summer NAO. Two empirical models are established to predict the strength of EASM based on the spring NAO. These equations correspond to the same-sign and opposite-sign scenarios, respectively, and are expressed as follows:

$$\mathrm{EASM}_{\mathrm{em}}|_{\text{same-sign}} = 0.44\mathrm{NAO} - 0.27 \quad \text{and} \tag{6}$$

$$\mathrm{EASM}_{\mathrm{em}}|_{\text{opposite-sign}} = 0.24\mathrm{NAO} + 0.18, \tag{7}$$

where $\mathrm{EASM}_{\mathrm{em}}$ represents the EASM index estimated by the empirical model. As discussed above, there are 16 same-sign years and 18 opposite-sign years. Only the first 13 yr from the corresponding scenarios are used to estimate the regression coefficients in Eqs. (6) and (7). Therefore, the first 13 yr act as a training period. The residual years (3 and 5 yr for the same-sign and opposite-sign scenarios, respectively) can be viewed as an independent testing period, because data from this period are not used in the calculation of model coefficients.

The levels of model performance for the same-sign and opposite-sign scenarios are shown in Figs. 13a and 13b, respectively. Red and black lines indicate the model-estimated and the observed EASM indices, respectively. It can be seen in Fig. 13a that the model in the

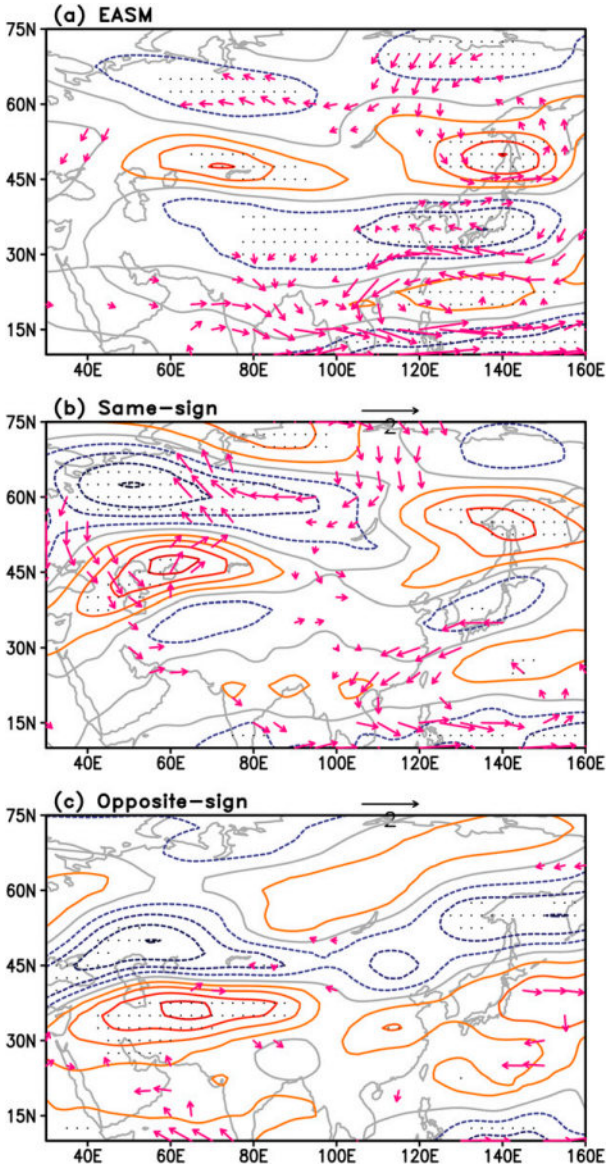

FIG. 12. Regression of zonal wind (contour interval = 0.5 m s^{-1}) at 200 hPa and horizontal wind (vectors; m s^{-1}) at 850 hPa against the (a) EASM, (b) spring-NAO index for the same-sign scenario, and (c) spring-NAO index for the opposite-sign scenario. The solid orange, dashed blue, and gray contours denote positive, negative, and zero regression-coefficient values, respectively. The stippling and red vectors represent statistical significance at the 90% confidence level for the contours and vectors, respectively.

same-sign scenario generally captures variations in the observed EASM index during the training period, with a correlation coefficient during this period of 0.44. During the independent testing period, the correlation coefficients for the model output and observations is 0.98. Although there are only three cases in this period, Fig. 13a shows that the model indeed offers a relatively accurate prediction of the EASM. In the opposite-sign scenario, the model performance is poor (Fig. 13b). In the training period, the correlation between the model-estimated and observed EASM indices is only 0.22. In the independent testing period, the correlation even becomes negative (−0.55). It is clear in Fig. 13b that the model forecast cannot capture the observed EASM index. The results in Fig. 13 illustrate that the prediction skill for the EASM based on the spring NAO is affected by the summer NAO.

It is well known that ENSO plays an important role in influencing the EASM, during both its decay and development phases (e.g., Fu and Teng 1988; Weng et al. 1999; Chang et al. 2000a, 2000b; Wang et al. 2000, 2008; Yang and Lau 2006; Wu et al. 2009; An et al. 2015). Two empirical seasonal prediction models based on the spring NAO and ENSO are developed using a multiple linear regression method for the same-sign and opposite-sign scenarios, respectively. These models are expressed as follows:

$$\mathrm{EASM}_{\mathrm{em}}|_{\text{same-sign}} = 0.30\mathrm{NAO} + 0.83\mathrm{ENSO}_{\mathrm{develop}} + 0.26\mathrm{ENSO}_{\mathrm{decay}} - 0.29 \quad (8)$$

and

$$\mathrm{EASM}_{\mathrm{em}}|_{\text{opposite-sign}} = 0.27\mathrm{NAO} - 0.03\mathrm{ENSO}_{\mathrm{develop}} - 0.58\mathrm{ENSO}_{\mathrm{decay}} + 0.13, \quad (9)$$

where $\mathrm{ENSO}_{\mathrm{decay}}$ denotes the Niño-3.4 index for the preceding winter (December–February) and $\mathrm{ENSO}_{\mathrm{develop}}$ denotes the Niño-3.4 index difference between April–May and February–March (the former minus the latter). As above, only the first 13 yr are used to estimate the regression coefficients in Eqs. (8) and (9), and the residual years can be viewed as an independent testing period.

The results from these two models are shown in Figs. 13a,b (blue lines). A comparison between Figs. 13a and 13b suggests that even if ENSO signals are included in the model, the model performance for the opposite-sign scenario is still weaker than the same-sign scenario. This is particularly evident in the independent testing period, where the correlations between the model results and the observed EASM indices are 0.76 in the same-sign scenario and only 0.03 in the opposite-sign scenario. This result indicates that the prediction skill for the EASM based on the spring NAO is affected by the summer NAO. In years when the polarities of the spring and summer NAO are the same, the EASM prediction based on the spring NAO tends to have better skill.

5. Discussion and conclusions

The influence of the NAO on the contemporaneous North Atlantic SST is mainly manifested as a tripolar pattern, known as the NAST. Previous studies have

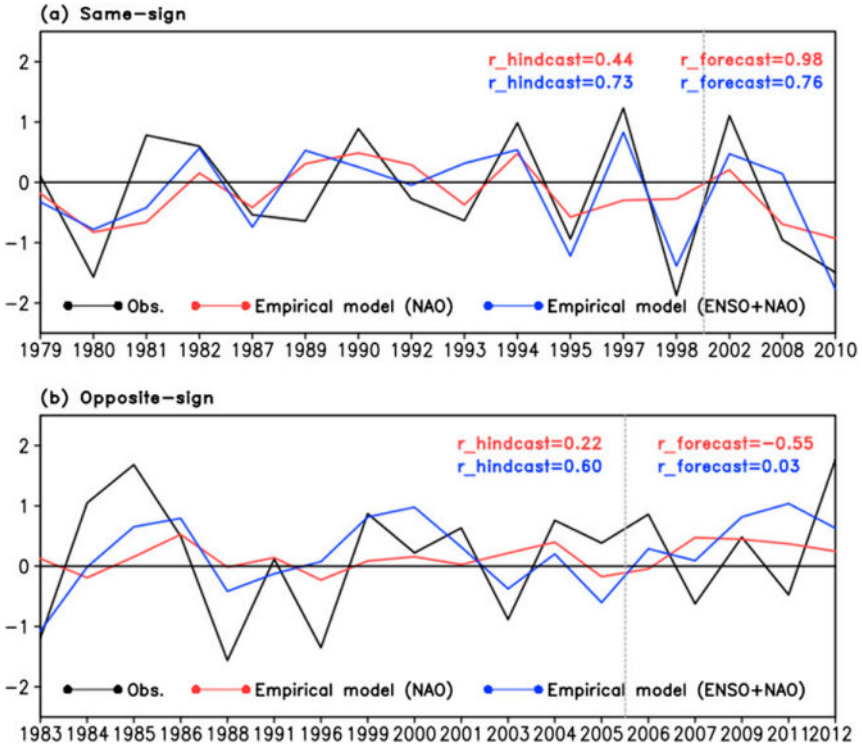

FIG. 13. EASM indices derived from observations (black line), an empirical model based on the spring NAO (red line), and that based on both the spring NAO and ENSO developing and decaying phases (blue line) for the (a) same-sign and (b) opposite-sign scenarios. The vertical gray dashed line distinguishes the training (hindcast) and testing (forecast) periods. The correlation coefficients between the observed EASM index and those from empirical models during the two periods are labeled at the top of the panels, with the red and blue colors representing NAO-based and NAO–ENSO-based models, respectively.

shown that the summer NAST is caused mainly by the preceding spring NAO, while the contemporaneous summer NAO plays a secondary role. The results of this study show that even if the summer NAO plays a secondary role, it may still perturb the summer SST anomalies caused by the spring NAO. The summer NAO perturbation of the spring-NAO-based EASM predictability is summarized in Fig. 14, which is divided into two scenarios. If the spring and summer NAOs have the same (opposite) polarity, the summer NAST pattern resulting from the spring NAO tends to be enhanced (reduced and changed to a quadrupolar pattern) by the summer NAO, which leads to a stronger (weaker) AEA teleconnection and thus stronger cyclonic circulation anomalies over the Ural Mountains. This scenario favors (does not favor) a weakened East Asian subtropical jet and results in a stronger (weaker) positive correlation between the spring NAO and EASM. Consequently, in years when the spring and summer NAO polarities are the same (opposite), EASM prediction based on the spring NAO tends to have better (limited) skill. The above results imply that consideration of the evolution of the NAO may provide useful information for EASM predictions. Special attention is required when there is a clear reversal in the polarity of the NAO, because the spring-NAO-based EASM predictability may be impaired in this situation by the opposite-sign summer NAO.

Since the EASM plays a critical role in regulating East Asian summer precipitation, the spring NAO could regulate East Asian summer rainfall by influencing the EASM (Wu et al. 2009, 2012; Zuo et al. 2012, 2013; Li et al. 2013). For example, a positive (negative) spring NAO tends to induce a strong (weak) monsoon year associated with a summer drought (flood) in the Yangtze River valley (e.g., Wang et al. 2000, 2008; Wu et al. 2009). Floods and droughts that occur in the Yangtze River valley in the summer season (June–August) in association with summer rainfall anomalies have a great impact on the infrastructure and economic development in this region. Accurate predictions of summer rainfall are thus of great importance to society. When the summer NAO has the same polarity as the spring NAO, the correlation between the spring NAO and summer rainfall in the middle and lower reaches of the Yangtze

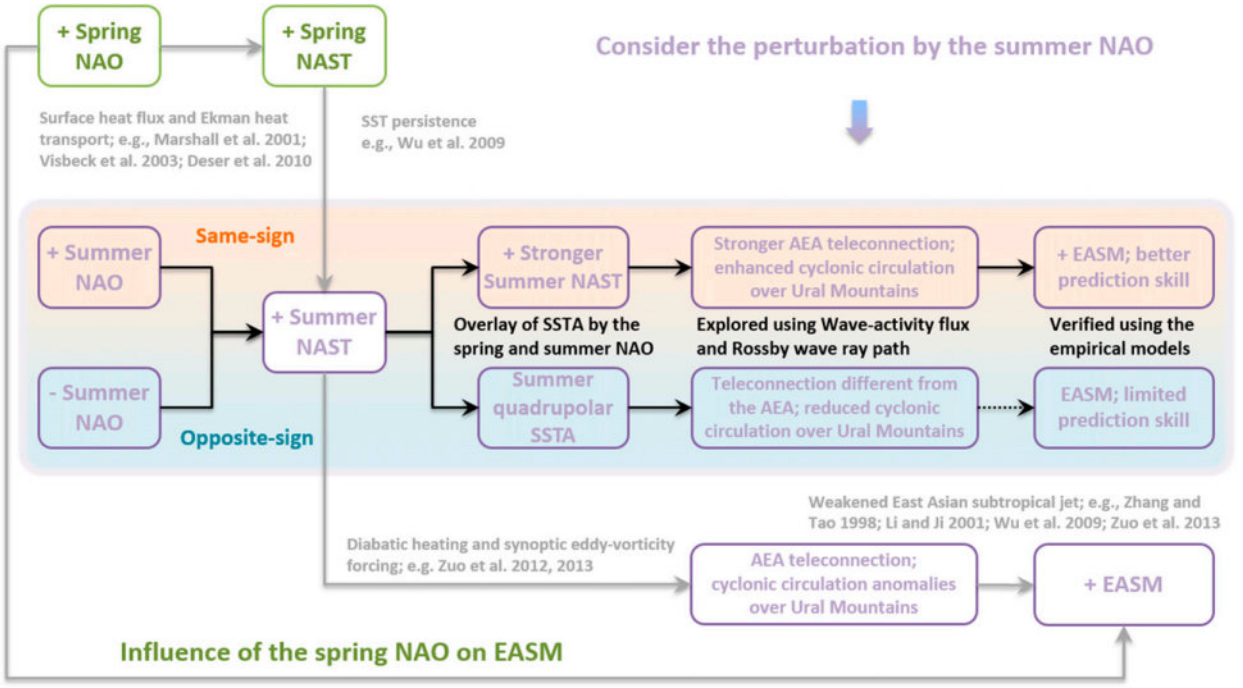

FIG. 14. Schematic showing perturbation of the summer NAO on the spring-NAO-based predictability of EASM. The green- and purple-lettered frames represent elements in spring and summer, respectively. The gray arrows represent the influence of the spring NAO on the EASM. Black arrows indicate perturbations by the summer NAO (shaded box).

River is stronger than in the opposite-sign scenario (not shown). Therefore, considering the evolution of the NAO is also helpful in terms of predicting summer monsoon rainfall based on the spring NAO.

The spatial and temporal variabilities of the EASM are very complex. In view of the role of the NAO and ENSO in influencing the EASM, their interactions may also regulate the skill in predicting the EASM (Wu and Lin 2012). It is worth noting that a mega-ENSO (Wang et al. 2013), which reflects a broader range of variability than the typical ENSO, may also interact with the NAO (Wu and Zhang 2015). Using a mega-ENSO as a predictor, Wu and Yu (2015) proposed a partial-least squares regression model as an effective method for establishing a physical–empirical model for the EASM.

Growing efforts have been focused on utilizing extratropical atmospheric circulation to conduct seasonal predictions (Rodwell and Folland 2002; Wu et al. 2009; Chen et al. 2013). Aside from the NAO, other extratropical atmospheric modes except for the NAO also imprint their signals on extratropical SST, and thus provide some predictability for climate in the following seasons via SST persistence (Nan and Li 2003; Nan et al. 2009; Zheng et al. 2015a). However, SST anomalies caused by the preceding atmospheric signal may be perturbed by the contemporaneous atmospheric signal, and these interactions may in turn affect seasonal predictions. The results of the present study indicate that it is necessary to pay attention to the evolution of extratropical atmospheric modes when carrying out seasonal predictions based on these extratropical modes.

Acknowledgments. This work was jointly supported by the 973 Program (2013CB430200) and the NSFC Project (41405086), as well as the China Special Fund for Meteorological Research in the Public Interest (GYHY201306031). Atmospheric circulation data were obtained from the NCEP–NCAR reanalysis (http://www.esrl.noaa.gov/psd/data/reanalysis/reanalysis.shtml). The SST dataset is the NOAA ERSST V3b (http://www.esrl.noaa.gov/psd/data/gridded/data.noaa.ersst.html). The monthly Niño-3.4 index is from the NOAA/CPC (http://www.cpc.ncep.noaa.gov/data/indices/). The authors appreciate valuable comments and suggestions from the editor and reviewers that have greatly assisted in improving the manuscript.

REFERENCES

An, Z. S., and Coauthors, 2015: Global monsoon dynamics and climate change. *Annu. Rev. Earth Planet. Sci.*, **43**, 29–77, doi:10.1146/annurev-earth-060313-054623.

Barnston, A. G., and R. E. Livezey, 1987: Classification, seasonality and persistence of low-frequency atmospheric circulation

patterns. *Mon. Wea. Rev.*, **115**, 1083–1126, doi:10.1175/1520-0493(1987)115<1083:CSAPOL>2.0.CO;2.

Chang, C.-P., Y. Zhang, and T. Li, 2000a: Interannual and interdecadal variation of the East Asian summer monsoon rainfall and tropical SSTs. Part I: Roles of the subtropical ridge. *J. Climate*, **13**, 4310–4325, doi:10.1175/1520-0442(2000)013<4310:IAIVOT>2.0.CO;2.

——, ——, and ——, 2000b: Interannual and interdecadal variation of the East Asian summer monsoon rainfall and tropical SSTs. Part II: Meridional structure of the monsoon. *J. Climate*, **13**, 4326–4340, doi:10.1175/1520-0442(2000)013<4326:IAIVOT>2.0.CO;2.

Chen, F. H., and Coauthors, 2015: East Asian summer monsoon precipitation variability since the last deglaciation. *Sci. Rep.*, **5**, 11186, doi:10.1038/srep11186.

Chen, L. J., Y. Yuan, M. Z. Yang, J. Q. Zuo, and W. J. Li, 2013: A review of physical mechanisms of the global SSTA impact on EASM. *J. Appl. Meteor. Sci.*, **5**, 521–532.

Chen, W., 1982: Fluctuations in Northern Hemisphere 700 mb height field associated with the Southern Oscillation. *Mon. Wea. Rev.*, **110**, 808–823, doi:10.1175/1520-0493(1982)110<0808:FINHMH>2.0.CO;2.

Davis, R. E., 1976: Predictability of sea surface temperature and sea level pressure anomalies over the North Pacific Ocean. *J. Phys. Oceanogr.*, **6**, 249–266, doi:10.1175/1520-0485(1976)006<0249:POSSTA>2.0.CO;2.

Deser, C., M. A. Alexander, and M. S. Timlin, 2003: Understanding the persistence of sea surface temperature anomalies in midlatitudes. *J. Climate*, **16**, 57–72, doi:10.1175/1520-0442(2003)016<0057:UTPOSS>2.0.CO;2.

——, ——, S.-P. Xie, and A. S. Phillips, 2010: Sea surface temperature variability: Patterns and mechanisms. *Annu. Rev. Mar. Sci.*, **2**, 115–143, doi:10.1146/annurev-marine-120408-151453.

Ding, Y. H., and J. C. L. Chan, 2005: The East Asian summer monsoon: An overview. *Meteor. Atmos. Phys.*, **89**, 117–142, doi:10.1007/s00703-005-0125-z.

Feng, J., J. Li, and Y. Li, 2010: A monsoon-like southwest Australian circulation and its relation with rainfall in southwest Western Australia. *J. Climate*, **23**, 1334–1353, doi:10.1175/2009JCLI2837.1.

——, ——, ——, J. L. Zhu, and F. Xie, 2015: Relationships among the monsoon-like southwest Australian circulation, the southern annular mode, and winter rainfall over southwest Western Australia. *Adv. Atmos. Sci.*, **32**, 1063–1076, doi:10.1007/s00376-014-4142-z.

Frederiksen, J. S., and P. J. Webster, 1988: Alternative theories of atmospheric teleconnections and low-frequency fluctuations. *Rev. Geophys.*, **26**, 459–494, doi:10.1029/RG026i003p00459.

Fu, C. B., and X. L. Teng, 1988: Relationship between summer climate in China and El Niño/Southern Oscillation phenomenon (in Chinese). *Chin. J. Atmos. Sci.*, **12**, 133–141.

Gong, D. Y., and S. W. Wang, 1999: Definition of Antarctic Oscillation index. *Geophys. Res. Lett.*, **26**, 459–462, doi:10.1029/1999GL900003.

——, J. Yang, S. J. Kim, Y. Q. Gao, D. Guo, T. J. Zhou, and M. Hu, 2011: Spring Arctic Oscillation-East Asian summer monsoon connection through circulation changes over the western North Pacific. *Climate Dyn.*, **37**, 2199–2216, doi:10.1007/s00382-011-1041-1.

Hartmann, D. L., and F. Lo, 1998: Wave-driven zonal flow vacillation in the Southern Hemisphere. *J. Atmos. Sci.*, **55**, 1303–1315, doi:10.1175/1520-0469(1998)055<1303:WDZFVI>2.0.CO;2.

Li, J., and Q. Zeng, 2000: Significance of the normalized seasonality of wind field and its rationality for characterizing the monsoon. *Sci. China*, **43D**, 646–653.

——, and ——, 2002: A unified monsoon index. *Geophys. Res. Lett.*, **29**, doi:10.1029/2001GL013874.

——, and J. X. L. Wang, 2003a: A modified zonal index and its physical sense. *Geophys. Res. Lett.*, **30**, 343–348, doi:10.1007/BF02690792.

——, and ——, 2003b: A new North Atlantic Oscillation index and its variability. *Adv. Atmos. Sci.*, **20**, 661–676, doi:10.1007/BF02690792.

——, and Coauthors, 2013: Progress in air–land–sea interactions in Asia and their role in global and Asian climate change. *Chin. J. Atmos. Sci.*, **37**, 518–538.

Li, S., and L. Ji, 2001: Background circulation characteristics of the persistence anomalies of the summertime circulation over the Ural Mountains (in Chinese). *Acta Meteor. Sin.*, **59**, 280–293.

Li, Y. J., J. Li, F. F. Jin, and S. Zhao, 2015: Interhemispheric propagation of stationary Rossby waves in a horizontally nonuniform background flow. *J. Atmos. Sci.*, **72**, 3233–3256, doi:10.1175/JAS-D-14-0239.1.

Lighthill, J., 1978: *Waves in Fluids.* Cambridge University Press, 504 pp.

Liu, Z., and M. Alexander, 2007: Atmospheric bridge, oceanic tunnel, and global climatic teleconnections. *Rev. Geophys.*, **45**, RG2005, doi:10.1029/2005RG000172.

Marshall, J., H. Johnson, and J. Goodman, 2001: A study of the interaction of the North Atlantic Oscillation with ocean circulation. *J. Climate*, **14**, 1399–1421, doi:10.1175/1520-0442(2001)014<1399:ASOTIO>2.0.CO;2.

Nan, S., and J. Li, 2003: The relationship between the summer precipitation in the Yangtze River valley and the boreal spring Southern Hemisphere annular mode. *Geophys. Res. Lett.*, **30**, 2266, doi:10.1029/2003GL018381.

——, ——, X. Yuan, and P. Zhao, 2009: Boreal spring Southern Hemisphere annular mode, Indian Ocean sea surface temperature, and East Asian summer monsoon. *J. Geophys. Res.*, **114**, D02103, doi:10.1029/2008JD010045.

Pan, L., 2005: Observed positive feedback between the NAO and the North Atlantic SSTA tripole. *Geophys. Res. Lett.*, **32**, L06707, doi:10.1029/2005GL022427.

Rodwell, M. J., and C. K. Folland, 2002: Atlantic air–sea interaction and seasonal predictability. *Quart. J. Roy. Meteor. Soc.*, **128**, 1413–1443, doi:10.1002/qj.200212858302.

Shi, F., S., J. Li, and R. J. S. Wilson, 2014: A tree-ring reconstruction of the South Asian summer monsoon index over the past millennium. *Sci. Rep.*, **4**, 6739, doi:10.1038/srep06739.

Takaya, K., and H. Nakamura, 2001: A formulation of a phase-independent wave-activity flux for stationary and migratory quasigeostrophic eddies on a zonally varying basic flow. *J. Atmos. Sci.*, **58**, 608–627, doi:10.1175/1520-0469(2001)058<0608:AFOAPI>2.0.CO;2.

Thompson, D. W. J., and J. M. Wallace, 2000: Annular modes in the extratropical circulation. Part I: Month-to-month variability. *J. Climate*, **13**, 1000–1016, doi:10.1175/1520-0442(2000)013<1000:AMITEC>2.0.CO;2.

Trenberth, K. E., G. W. Branstator, D. Karoly, A. Kumar, N.-C. Lau, and C. Ropelewski, 1998: Progress during TOGA in understanding and modeling global teleconnections associated with tropical sea surface temperatures. *J. Geophys. Res.*, **103**, 14 291–14 324, doi:10.1029/97JC01444.

Van Loon, H., and J. C. Rogers, 1978: The seesaw in winter temperatures between Greenland and northern Europe. Part I:

General description. *Mon. Wea. Rev.*, **106**, 296–310, doi:10.1175/1520-0493(1978)106<0296:TSIWTB>2.0.CO;2.

Visbeck, M, E. P. Chassignet, R. G. Curry, T. L. Delworth, R. R. Dickson, and K. Krahmann, 2003: The ocean's response to North Atlantic Oscillation variability. *The North Atlantic Oscillation: Climatic Significance and Environmental Impact*, *Geophys. Monogr.*, Vol. 134, Amer. Geophys. Union, 113–146, doi:10.1029/134GM06.

Wang, B., and Z. Fan, 1999: Choice of South Asian summer monsoon indices. *Bull. Amer. Meteor. Soc.*, **80**, 629–638, doi:10.1175/1520-0477(1999)080<0629:COSASM>2.0.CO;2.

——, R. Wu, and X. Fu, 2000: Pacific–East Asian teleconnection: How does ENSO affect East Asian climate? *J. Climate*, **13**, 1517–1536, doi:10.1175/1520-0442(2000)013<1517:PEATHD>2.0.CO;2.

——, Z. Wu, J. Li, J. Liu, C.-P. Chang, Y. Ding, and G. Wu, 2008: How to measure the strength of the East Asian summer monsoon? *J. Climate*, **21**, 4449–4463, doi:10.1175/2008JCLI2183.1.

——, J. Liu, H. J. Kim, P. J. Webster, S. Y. Yim, and B. Q. Xiang, 2013: Northern Hemisphere summer monsoon intensified by mega-El Niño/southern oscillation and Atlantic multidecadal oscillation. *Proc. Natl. Acad. Sci. USA*, **110**, 5347–5352, doi:10.1073/pnas.1219405110.

Wang, H. J., 2001: The weakening of the Asian monsoon circulation after the end of 1970's. *Adv. Atmos. Sci.*, **18**, 376–386, doi:10.1007/BF02919316.

Weng, H. Y., K. M. Lau, and Y. Xue, 1999: Multi-scale summer rainfall variability over China and its long-term link to global sea surface temperature variability. *J. Meteor. Soc. Japan*, **77**, 845–857.

Wu, Z., and H. Lin, 2012: Interdecadal variability of the ENSO–North Atlantic Oscillation connection in boreal summer. *Quart. J. Roy. Meteor. Soc.*, **138**, 1668–1675, doi:10.1002/qj.1889.

——, and L. Yu, 2015: Seasonal prediction of the East Asian summer monsoon with a partial-least square model. *Climate Dyn.*, **46**, 3067–3078, doi:10.1007/s00382-015-2753-4.

——, and P. Zhang, 2015: Interdecadal variability of the mega-ENSO–NAO synchronization in winter. *Climate Dyn.*, **45**, 1117–1128, doi:10.1007/s00382-014-2361-8.

——, B. Wang, J. Li, and F. F. Jin, 2009: An empirical seasonal prediction model of the East Asian summer monsoon using ENSO and NAO. *J. Geophys. Res.*, **114**, D18120, doi:10.1029/2009JD011733.

——, J. P. Li, Z. Jiang, J. He, and X. Zhu, 2012: Possible effects of the North Atlantic Oscillation on the strengthening relationship between the East Asian summer monsoon and ENSO. *Int. J. Climatol.*, **32**, 794–800, doi:10.1002/joc.2309.

Xie, S. P., 2004: Satellite observations of cool ocean–atmosphere interaction. *Bull. Amer. Meteor. Soc.*, **85**, 195–208, doi:10.1175/BAMS-85-2-195.

Xu, H., J. Feng, and C. Sun, 2013: Impact of preceding summer North Atlantic Oscillation on early autumn precipitation over central China. *Atmos. Ocean. Sci. Lett.*, **6**, 417–422, doi:10.3878/j.issn.1674-2834.13.0027.

Yang, S., and K.-M. Lau, 2006: Interannual variability of the Asian monsoon. *The Asian Monsoon*, B. Wang, Ed., Springer, 259–293.

Zhang, Q. Y., and S. Y. Tao, 1998: Influence of Asian mid-latitude circulation on East Asian summer rainfall (in Chinese). *Acta Meteor. Sin.*, **56**, 199–211.

Zhao, S., J. Li, and Y. J. Li, 2015: Dynamics of an interhemispheric teleconnection across the critical latitude through a southerly duct during boreal winter. *J. Climate*, **28**, 7437–7456, doi:10.1175/JCLI-D-14-00425.1.

Zheng, F., J. P. Li, J. Feng, Y. J. Li, and Y. Li, 2015a: Relative importance of the austral summer and autumn SAM in modulating Southern Hemisphere extratropical autumn SST. *J. Climate*, **28**, 8003–8020, doi:10.1175/JCLI-D-15-0170.1.

——, ——, L. Wang, F. Xie, and X. F. Li, 2015b: Cross-seasonal influence of the December–February Southern Hemisphere annular mode on March–May meridional circulation and precipitation. *J. Climate*, **28**, 6859–6881, doi:10.1175/JCLI-D-14-00515.1.

Zuo, J. Q., W. J. Li, H. L. Ren, and L. J. Chen, 2012: Change of the relationship between the spring NAO and East Asian summer monsoon and its possible mechanism. *Chin. J. Geophys.*, **55**, 23–34, doi:10.1002/cjg2.1697.

——, ——, C. H. Sun, L. Xu, and H. L. Ren, 2013: Impact of the North Atlantic sea surface temperature tripole on the East Asian summer monsoon. *Adv. Atmos. Sci.*, **30**, 1173–1186, doi:10.1007/s00376-012-2125-5.